(Preprint) AAS 17-613

A NEW CONCEPT OF STABILITY IN ORBIT PROPAGATION, USEFUL FOR QUANTIFYING NUMERICAL ERRORS

Javier Roa[*], Hodei Urrutxua[†] and Jesús Peláez[‡]

We present the concept of topological stability in the numerical propagation of orbits, and show how it results in a useful new method for measuring the global numerical error of an orbit propagation. The concept applies to any problem in orbital dynamics. Moreover, it can be extended to any three-dimensional system of differential equations of second order. In order to assess the topological stability of a given integration a special metric is introduced, which can be used to estimate the numerical errors robustly. The method is particularly well suited for dealing with strongly perturbed and chaotic systems. The construction is based on the constraint imposed by the Hopf map that supports the Kustaanheimo-Stiefel transformation. Generic concepts of stability are translated to KS space.

INTRODUCTION

The theoretical development in the present paper provides a practical technique for measuring the global error in the numerical propagation of a given orbit. The next section explains the algorithm in a self-contained way. The method stems from the new concept of *topological stability*, which relates to how well the topological structure of the Kustaanheimo-Stiefel (KS) space is preserved during the integration.

The connection between the KS transformation and the Hopf map reveals why four dimensions are required to regularize three-dimensional motion. The extra dimension, represented by a Hopf fibration, introduces a degree of freedom in the problem. The solution to three-dimensional motion is no longer unique, as there are now infinitely many trajectories in KS space that depart with the same exact initial conditions $\mathbf{r}_0$ and $\mathbf{v}_0$. Realizing that all trajectories originating from the same fiber should represent the same solution in Cartesian space imposes new constraints on the propagation of the orbit, and results in the concept of topological stability.

There are different methods available for measuring the accuracy of the propagation. If the system admits conservation laws, checking how well they are actually conserved is often a good indicator of accuracy. However, there are problems in which the energy is well conserved while errors in position and velocity are significant (we will show an example of such system in the last section). When the propagator is written in a programming language that supports extended floating-point precision (beyond double), it might be possible to generate a very accurate solution by using high-order integrators and reducing the step-size significantly. But this option is not always available. An alternative error metric consists in propagating the orbit forward in time and then backward,

[*]Post-doctoral Fellow, Solar System Dynamics Group. Jet Propulsion Laboratory, California Institute of Technology, Pasadena, CA 91109, USA. Member AIAA, javier.roa@jpl.nasa.gov.
[†]New Frontiers Fellow, Astronautics Research Group, University of Southampton, Southampton SO17 1BJ, UK.
[‡]Professor and Head, Space Dynamics Group, Technical University of Madrid, Madrid, Spain, E-28040.

evaluating how close the final state is compared to its initial value. This technique might represent the global error, although it depends on the time-reversibility properties of the integrator. There are still no portable, robust, and standard methods for evaluating the accuracy of generic propagations.

This paper present a method to solve this particular problem using a compact algorithm. The theoretical foundations are presented in the following sections, including fundamental concepts like the manifold of solutions and $\mathscr{K}$-separation. Then, the algorithm is summarized from a practical perspective. The final section of the paper discusses the applicability of the method through a number of examples.

THE KS TRANSFORMATION AS A HOPF MAP

Let $\mathbf{r} = (x, y, z)^\top$ be the position vector of a point in Cartesian space $\mathbb{E}^3$, projected in an inertial frame $\Im$, and let $\mathbf{x} = (x, y, z, 0)^\top$ be its extension to $\mathbb{R}^4$. Kustaanheimo and Stiefel[1] found a regularization of the two-body problem introducing the new coordinates $\mathbf{u} = (u_1, u_2, u_3, u_4)^\top$, defined in the parametric space $\mathbb{U}^4$ embedded in $\mathbb{R}^4$. The KS transformation is defined explicitly as

$$\mathbf{x} = \mathscr{K}(\mathbf{u}) = \mathsf{L}(\mathbf{u})\,\mathbf{u}, \tag{1}$$

where $\mathsf{L}(\mathbf{u})$ is known as the KS matrix:

$$\mathsf{L}(\mathbf{u}) = \begin{bmatrix} u_1 & -u_2 & -u_3 & u_4 \\ u_2 & u_1 & -u_4 & -u_3 \\ u_3 & u_4 & u_1 & u_2 \\ u_4 & -u_3 & u_2 & -u_1 \end{bmatrix}.$$

The KS matrix is r-orthogonal, i.e.

$$\mathsf{L}^{-1}(\mathbf{u}) = \frac{1}{r}\,\mathsf{L}^\top(\mathbf{u}). \tag{2}$$

Every point $\mathbf{u}$ is KS-mapped to one single point in Cartesian space $\mathbb{E}^3$. These equations are a particular case of the more general map proposed by Hopf.[2]

Regularizing the equations of orbital motion by means of the KS transformation requires the time transformation due to Sundman:[3]

$$\mathrm{d}t = r\,\mathrm{d}s, \tag{3}$$

where s is referred to as the fictitious time, and $r = \|\mathbf{r}\|$. Derivatives with respect to physical time t will be denoted by a dot, $\dot{\mathbf{r}}$, whereas derivatives with respect to fictitious time will be written $\mathbf{r}'$. The radial distance r relates to KS variables by means of

$$r = u_1^2 + u_2^2 + u_3^2 + u_4^2 = \|\mathbf{u}\|^2. \tag{4}$$

The KS transformation maps fibers on the 3-sphere of radius $\sqrt{r}$ in $\mathbb{U}^4$ to points on the 2-sphere of radius r in $\mathbb{E}^3$.

Hopf[2] proved that the transformation from the 3-sphere to the 2-sphere maps circles to single points, defining the structure $\mathbb{S}^1 \hookrightarrow \mathbb{S}^3 \to \mathbb{S}^2$. Equation (1) is invariant under the gauge transformation $\mathscr{R} : \mathbf{u} \mapsto \mathbf{w}$,

$$\mathbf{x} = \mathsf{L}(\mathbf{u})\,\mathbf{u} = \mathsf{L}(\mathbf{w})\,\mathbf{w}. \tag{5}$$

Vector $\mathbf{w} = (w_1, w_2, w_3, w_4)^\top$ takes the form:

$$\mathbf{w} = \mathscr{R}(\vartheta; \mathbf{u}) = \mathsf{R}(\vartheta)\,\mathbf{u}, \tag{6}$$

where $\mathbf{R}(\vartheta)$ is the matrix

$$\mathbf{R}(\vartheta) = \begin{bmatrix} \cos\vartheta & 0 & 0 & -\sin\vartheta \\ 0 & \cos\vartheta & \sin\vartheta & 0 \\ 0 & -\sin\vartheta & \cos\vartheta & 0 \\ \sin\vartheta & 0 & 0 & \cos\vartheta \end{bmatrix}. \tag{7}$$

This matrix is orthogonal, and also

$$\mathbf{R}^{\top}(\vartheta) = \mathbf{R}(-\vartheta).$$

Being $\mathbf{R}(\vartheta)$ orthogonal Eq. (6) can be inverted to provide

$$\mathbf{u} = \mathscr{R}^{-1}(\vartheta; \mathbf{w}) = \mathbf{R}(-\vartheta)\,\mathbf{w}. \tag{8}$$

The transformation $\mathscr{R}$ preserves the radius r, i.e.

$$r = \mathbf{u}\cdot\mathbf{u} = \mathbf{w}\cdot\mathbf{w}.$$

Since the radius is invariant to the selection of the point in the fiber it follows that the physical time, defined by Eq. (3), is $\mathscr{R}$-invariant as well*. The identity in Eq. (5) and the r-orthogonality of matrix $\mathbf{L}$ furnish a useful relation:

$$\mathbf{w} = \mathbf{L}^{-1}(\mathbf{w})\,\mathbf{L}(\mathbf{u})\,\mathbf{u} = \mathbf{R}(\vartheta)\,\mathbf{u} \implies \mathbf{L}^{\top}(\mathbf{w})\,\mathbf{L}(\mathbf{u}) = r\mathbf{R}(\vartheta).$$

The angular variable ϑ parameterizes the Hopf fibration in four-dimensional space. In fact, Eq. (6) defines explicitly the fiber $\mathcal{F}$: changing the value of ϑ defines different points in $\mathbb{U}^4$ that are KS transformed to the same point in $\mathbb{E}^3$. This yields the definition of fiber as the subset of all points in four-dimensional space that are mapped into the same point in $\mathbb{E}^3$ by means of the KS transformation,

$$\mathcal{F} = \{\mathbf{w}(\vartheta) \in \mathbb{U}^4 \,\big|\, \mathbf{x} = \mathscr{K}(\mathbf{w}),\ \forall\vartheta \in [0, 2\pi]\}.$$

A different fiber transforms into a different point. Consequently, two fibers cannot intersect because the intersection point will then be transformed into the same point in $\mathbb{E}^3$ despite belonging to two different fibers.[6] The stereographic projection of the fibers onto $\mathbb{E}^3$ reveals that two fibers in KS space are connected by a Hopf link, as sketched in Fig. 1.

Figure 1: **Hopf link connecting two different fibers in KS space, visualized by means of the stereographic projection to $\mathbb{E}^3$**

The velocity and the bilinear relation

Let $\mathbf{u}, \mathbf{w} \in \mathbb{U}^4$. The KS matrix satisfies the property

$$\mathbf{L}(\mathbf{u})\,\mathbf{w} = \mathbf{L}(\mathbf{w})\,\mathbf{u} \iff \ell(\mathbf{u}, \mathbf{w}) = 0,$$

*Alternative forms of the time transformation can be found in the literature, generalized as $\mathrm{d}t/\mathrm{d}s = g(\mathbf{x}, \dot{\mathbf{x}})$. We refer to the work by Zare and Szebehely[4] for a survey of transformations involving different powers of the radial distance, the potential, the Lagrangian, or combinations of the relative separations for the case of N-body problems. The vectors $\mathbf{x}$ and $\dot{\mathbf{x}}$ are $\mathscr{R}$-invariant, so the uniqueness of the physical time is also guaranteed for more general transformations.[5]

where $\ell(\mathbf{u}, \mathbf{w})$ denotes the bilinear relation

$$\ell(\mathbf{u}, \mathbf{w}) = u_1 w_4 - u_2 w_3 + u_3 w_2 - u_4 w_1.$$

Differentiating Eq. (1) with respect to fictitious time and taking into account the time transformation from Eq. (3) yields

$$\dot{\mathbf{x}} = \frac{2}{r} \mathbf{L}(\mathbf{u})\, \mathbf{u}', \tag{9}$$

where $\dot{\mathbf{x}} = (v_x, v_y, v_z, 0)^\top$ is the velocity vector extended to $\mathbb{R}^4$. Note that the fourth component is zero, which means

$$\ell(\mathbf{u}, \mathbf{u}') = 0.$$

Moreover, Stiefel and Scheifele[6] proved that $\ell(\mathbf{u}, \mathbf{u}') = 0$ is a first integral of orbital motion. Provided that the KS transformation is $\mathscr{R}$-invariant, it follows that the bilinear relation holds for all points in a given fiber,

$$\ell(\mathbf{w}, \mathbf{w}') = \ell(\mathbf{u}, \mathbf{u}') = 0. \tag{10}$$

Let $\mathbf{t}(\vartheta) \in \mathbb{U}^4$ denote the vector that is tangent to a fiber $\mathcal{F}$ at $\mathbf{w}(\vartheta)$. The direction of $\mathbf{t}$ can be obtained by differentiating Eq. (6) with respect to ϑ. It reads

$$\mathbf{t} = \mathbf{R}^*(\vartheta)\, \mathbf{u}$$

where $\mathbf{R}^*(\vartheta) = \mathrm{d}\mathbf{R}(\vartheta)/\mathrm{d}\vartheta$ is obtained by differentiating Eq. (7). Taking as an example $\vartheta = 0$ yields the components of the tangent vector $\mathbf{t}$,

$$\mathbf{t} = (-u_4, u_3, -u_2, u_1)^\top \tag{11}$$

This unveils a geometric interpretation of the bilinear relation $\ell(\mathbf{u}, \mathbf{v}) = 0$: it can be understood as an orthogonality condition, since

$$\ell(\mathbf{u}, \mathbf{v}) = 0 \iff \mathbf{v} \cdot \mathbf{t} = 0.$$

Two vectors $\mathbf{u}$ and $\mathbf{v}$ satisfy the bilinear relation $\ell(\mathbf{u}, \mathbf{v}) = 0$ if $\mathbf{v}$ is orthogonal to the fiber through $\mathbf{u}$. Provided that $\ell(\mathbf{u}, \mathbf{u}') = 0$ holds naturally and it is an integral of motion it follows that the velocity in KS space, $\mathbf{u}'$, is always orthogonal to the fiber at $\mathbf{u}$. The fiber bundle $\mathcal{S}^1 \hookrightarrow \mathcal{S}^3 \to \mathcal{S}^2$ shows that the fibers constituting the 3-sphere are circles, corresponding to points on the 2-sphere. Indeed, the tangent vector $\mathbf{t}(\vartheta)$ is always perpendicular to the position vector $\mathbf{w}(\vartheta)$,

$$\mathbf{w} \cdot \mathbf{t} = [\mathbf{R}(\vartheta)\, \mathbf{u}] \cdot [\mathbf{R}^*(\vartheta)\, \mathbf{u}] = \mathbf{u} \cdot \left\{ \mathbf{R}^\top(\vartheta)\, [\mathbf{R}^*(\vartheta) \mathbf{u}] \right\} = 0$$

no matter the value of ϑ.

The inverse mapping

The inverse KS transformation $\mathscr{K}^{-1} : \mathbf{x} \mapsto \mathbf{u}$ maps points to fibers. Introducing the auxiliary vector $\mathbf{v} = (v_1, v_2, v_3, v_4)^\top$ the inverse mapping takes the form

$$\begin{aligned} v_1 &= R \sin\theta \\ v_2 &= \frac{1}{2R}(y \sin\theta - z \cos\theta) \\ v_3 &= \frac{1}{2R}(y \cos\theta + z \sin\theta) \\ v_4 &= -R \cos\theta. \end{aligned} \tag{12}$$

Here $R^2 = (r + |x|)/2$. The angle θ is different from ϑ: the points on the fiber are parameterized by θ, which is measured with respect to a certain axis; given two points $\mathbf{u}$ and $\mathbf{w}$ obtained by setting $\theta = \theta_1$ and θ_2 in Eq. (12), respectively, they relate by virtue of Eq. (6). This equation then provides the relation:

$$\theta_2 - \theta_1 = \vartheta$$

meaning that the variable ϑ denotes the angular *separation* between points along the same fiber. The value of θ depends on the position of the reference axis, whereas ϑ is independent from the selection of the axis.

The point $\mathbf{u}$ is finally defined as

$$\begin{aligned} \mathbf{u} &= (v_1, v_2, v_3, v_4)^\top \quad \text{if } x \geq 0 \\ \mathbf{u} &= (v_2, v_1, v_4, v_3)^\top \quad \text{if } x < 0. \end{aligned} \tag{13}$$

Two alternative expressions are considered for avoiding potential singularities. They differ in the selection of the axes in KS space. From this result any point $\mathbf{w}_0$ in the initial fiber $\mathcal{F}_0$ can be obtained from

$$\begin{aligned} \mathbf{w}_0(\vartheta) &= \mathbf{R}(\vartheta)\,\mathbf{u}_0 \qquad \text{if } x_0 \geq 0 \\ \mathbf{w}_0(\vartheta) &= \mathbf{R}(-\vartheta)\,\mathbf{u}_0 \qquad \text{if } x_0 < 0 \end{aligned} \tag{14}$$

so that $\mathbf{x}_0 = \mathbf{L}(\mathbf{w}_0)\mathbf{w}_0$. The sign criterion complies with the different definitions of the axes in KS space.

The velocity in $\mathbb{U}^4$ is obtained by inverting Eq. (9), taking into account the orthogonality relation in Eq. (2):

$$\mathbf{u}' = \frac{1}{2}\mathbf{L}^\top(\mathbf{u})\,\dot{\mathbf{x}}. \tag{15}$$

The geometry of the inverse KS transformation can be studied from Fig. 2. The gray sphere is three-dimensional and of radius r. The black arc corresponds to a set of initial conditions, $\mathbf{r}_j$. The white dot represents one particular position in $\mathbb{E}^3$, $\mathbf{r}_i$. The inverse KS transformation applied to $\mathbf{r}_i$ yields the fiber $\mathcal{F}_i$. The fiber is represented by means of its stereographic projection to $\mathbb{R}^3$. The black surface consists of all the fibers $\mathcal{F}_j$ that are KS mapped to the points $\mathbf{r}_j$. In this figure it is possible to observe the Hopf link connecting different fibers.

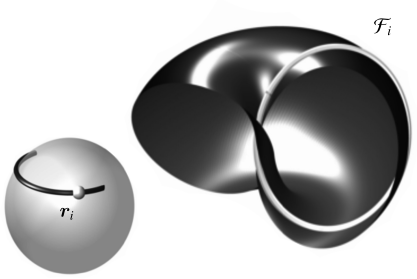

Figure 2: **Stereographic projection to $\mathbb{R}^3$ of the Hopf fibration corresponding to a set of initial positions on the three-dimensional sphere of radius r**

STABILITY IN KS SPACE

The classical concepts of stability from Lyapunov and Poincaré can be translated to KS language by considering the topology of the transformation. First, we introduce an important theorem regarding the geometry of the fibers. From this theorem the concept of the fundamental manifold arises naturally.

The stability concepts here presented are not based in numerical analyses; previous studies about the stability of KS transformation[7,8,9] focus on the behavior of the *numerical procedure*. We aim for a series of definitions that capture the *physical behavior*, which should be independent from the formulation of the dynamics.

A central theorem

Two fibers can never intersect, as discussed when formally defining a fiber. It is now possible to advance on this statement and to formulate a fundamental property of the KS transformation:

Theorem 1: *(Roa et al. 2016[10]) The angular separation between two trajectories emanating from $\mathcal{F}_0$, measured along every fiber, is constant. That is*

$$\mathbf{w}_0 = \mathbf{R}(\vartheta_0)\,\mathbf{u}_0 \implies \mathbf{w}(s) = \mathbf{R}(\vartheta_0)\,\mathbf{u}(s)$$

for any value of ϑ_0 and the fictitious time s. This is an intrinsic property of KS space and does not depend on the dynamics of the system.

Proof: Consider two trajectories in KS space, $\mathbf{u} = \mathbf{u}(s)$ and $\mathbf{w} = \mathbf{w}(s)$, departing from the same fiber $\mathcal{F}_0$. They relate by means of Eq. (6). In the most general case the angle ϑ can be described by a function $\vartheta = \vartheta(s)$ and initially it is $\vartheta(0) = \vartheta_0$. The trajectories evolve according to

$$\mathbf{w}(s) = \mathscr{R}(\vartheta; \mathbf{u}(s)) = \mathbf{R}(\vartheta)\mathbf{u}(s). \tag{16}$$

Differentiating this equation with respect to fictitious time yields

$$\mathbf{w}'(s) = \mathbf{R}'(\vartheta)\,\mathbf{u}(s) + \mathbf{R}(\vartheta)\,\mathbf{u}'(s). \tag{17}$$

Equation (10) proved that the bilinear relation holds for any trajectory in KS space, meaning that $\ell(\mathbf{w}, \mathbf{w}') = \ell(\mathbf{u}, \mathbf{u}') = 0$. This renders:

$$\ell(\mathbf{w}, \mathbf{w}') = \ell(\mathbf{R}(\vartheta)\mathbf{u}, \mathbf{R}'(\vartheta)\,\mathbf{u} + \mathbf{R}(\vartheta)\,\mathbf{u}') = 0$$

after substituting Eqs. (16) and (17). Expanding the bilinear relation in the previous expression shows that

$$\ell(\mathbf{R}(\vartheta)\mathbf{u}, \mathbf{R}'(\vartheta)\,\mathbf{u} + \mathbf{R}(\vartheta)\,\mathbf{u}') = r\,\frac{\mathrm{d}\vartheta}{\mathrm{d}s} + \ell(\mathbf{u}, \mathbf{u}') = 0.$$

Assuming that $r > 0$ and considering that $\ell(\mathbf{u}, \mathbf{u}') = 0$ one gets

$$\frac{\mathrm{d}\vartheta}{\mathrm{d}s} = 0 \implies \vartheta(s) = \vartheta_0$$

so the angular separation along every fiber remains constant. We emphasize that no assumptions about the dynamics have been made. ■

A direct consequence of this result is the relation between the velocities along the trajectories $\mathbf{u}(s)$ and $\mathbf{w}(s)$:

$$\mathbf{w}'(s) = \mathscr{R}(\vartheta; \mathbf{u}'(s)).$$

The fundamental manifold Γ

A trajectory in Cartesian space, understood as a continuum of points in $\mathbb{E}^3$, is represented by a continuum of fibers in $\mathbb{U}^4$. Each fiber is KS transformed to a point of the trajectory. The fibers form the *fundamental manifold*, Γ.

Equation (14) defines the initial fiber $\mathcal{F}_0$, which yields a whole family of solutions parameterized by the angular variable ϑ. Every trajectory $\mathbf{w}(s)$ is confined to the fundamental manifold. Thanks to Thm. 1 the manifold Γ can be constructed following a simple procedure: first, a reference trajectory $\mathbf{u}(s)$ is propagated from any point in $\mathcal{F}_0$; then, mapping the transformation $\mathscr{R}$ over it renders a fiber $\mathcal{F}_i$ for each point $\mathbf{u}(s_i)$ of the trajectory. The set $\cup_i \mathcal{F}_i$ defines Γ. Recall that

$$\bigcap_i \mathcal{F}_i = \emptyset.$$

The fact that all trajectories emanating from $\mathcal{F}_0$ are confined to Γ is what makes an arbitrary choice of θ in Eq. (12) possible. The diagram in Fig. 3 depicts the construction of the fundamental manifold Γ.

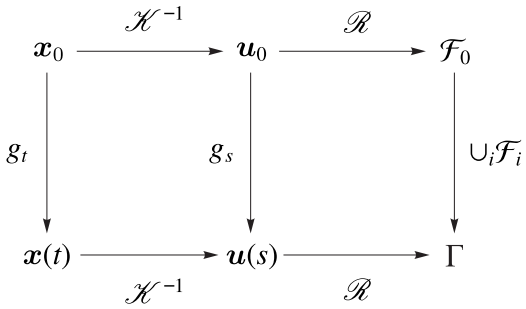

Figure 3: **Construction of the fundamental manifold: the mapping $g_t : \mathbf{x}_0 \mapsto \mathbf{x}(t)$ denotes the integration of the trajectory from t_0 to t, and g_s refers to the propagation using the fictitious time**

Fixed points, limit cycles and attractors

Points in $\mathbb{E}^3$ transform into fibers in $\mathbb{U}^4$. Thus, a fixed point in Cartesian space, $\mathbf{x}_0$, translates into a fixed fiber in KS space, $\mathcal{F}_0$. Asymptotically stable fixed fibers (to be defined formally in the next section) attract the fundamental manifold of solutions, $\Gamma \to \mathcal{F}_0$. Asymptotic instability is equivalent to the previous case under a time reversal.

Limit cycles are transformed to fundamental manifolds, referred to as limit fundamental manifolds Γ_0. A fundamental manifold Γ originating in the basin of attraction of a limit fundamental manifold will converge to it after sufficient time. For $\Gamma \to \Gamma_0$ convergence means that each fiber in Γ approaches the corresponding fiber in Γ_0. Correspondence between fibers is governed by the t-synchronism.

In a more general sense, attractors in $\mathbb{U}^4$ are invariant sets of the flow. The point-to-fiber correspondence connects attractors in $\mathbb{E}^3$ with attractors in KS space. The basin of attraction of an attractive set $Y_u \subset \mathbb{U}^4$ is built from its definition in three dimensions. Let $X \subset \mathbb{E}^3$ be the basin of attraction of Y. It can be transformed to KS space, $X \to X_u$, thanks to

$$X_u = (\mathscr{R} \circ \mathscr{K}^{-1})(X) = \mathscr{R}(\mathscr{K}^{-1}(X)).$$

This construction transforms arbitrary sets in $\mathbb{E}^3$ to $\mathbb{U}^4$. The inverse KS transformation constitutes a dimension raising mapping, so in general $\dim(X_u) = \dim(X) + 1$.

Relative dynamics and synchronism

The theories about the local stability of dynamical systems are based on the relative dynamics between nearby trajectories. The concepts of stability formalize how the separation between two (initially close) trajectories evolves in time. But the concept of *time evolution* requires a further discussion because of having introduced an alternative time variable via the Sundman transformation.

Keplerian motion is known to be Lyapunov unstable. Small differences in the semimajor axes of two orbits result in a separation that grows in time because of having different periods. However, Kepler's problem transforms into a harmonic oscillator by means of the KS transformation, with the fictitious time being equivalent to the eccentric anomaly. The resulting system is stable: for

fixed values of the eccentric anomaly the separation between points in each orbit will be small, because of the structural (or Poincaré) stability of the motion. These considerations are critical for the numerical integration of the equations of motion. But in this paper we seek a theory of stability in $\mathbb{U}^4$ expressed in the language of the physical time t, because of its physical and practical interest. The conclusions about the stability of the system will be equivalent to those obtained in Cartesian space.

The spectrum of the linearized form of Kepler's problem written in Cartesian coordinates,

$$\frac{\mathrm{d}^2\mathbf{r}}{\mathrm{d}\,t^2} = -\frac{\mathbf{r}}{r^3}$$

exhibits one eigenvalue with positive real part, $\lambda = \sqrt{2/r^3}$. Lyapunov's theory of linear stability states that the system is unstable.

Under the action of the KS transformation Kepler's problem transforms into

$$\frac{\mathrm{d}^2\mathbf{u}}{\mathrm{d}s^2} = -\frac{h}{2}\,\mathbf{u} \tag{18}$$

where h is minus the Keplerian energy. Although the linear analysis is not useful in this case, selecting a candidate Lyapunov function $V(\mathbf{u},\mathbf{u}') = h(\mathbf{u}\cdot\mathbf{u})/4 + (\mathbf{u}'\cdot\mathbf{u}')/2$ the stability of the system is proved. In order to represent the Lyapunov instability of the motion with respect to time t the Sundman transformation needs to be considered. Given two circular orbits of radii r_1 and r_2, the time delay between both solutions reads

$$\Delta t = t_2 - t_1 = (r_2 - r_1)s.$$

The time delay grows with fictitious time and small values of $r_2 - r_1$ do not guarantee that Δt remains small.

This phenomenon relates to the synchronism of the solutions.[11,12] Solutions to the system defined in Eq. (18) are stable if they are synchronized in fictitious time, but unstable if they are synchronized in physical time. We adopt this last form of synchronism for physical coherence.

Stability of the fundamental manifold

Lyapunov stability A trajectory $\mathbf{r}(t)$ in $\mathbb{E}^3$ is said to be Lyapunov stable if, for every small $\varepsilon > 0$, there is a value $\delta > 0$ such that for any other solution $\mathbf{r}^*(t)$ satisfying $\|\mathbf{r}(t_0) - \mathbf{r}^*(t_0)\| < \delta$ it is $\|\mathbf{r}(t) - \mathbf{r}^*(t)\| < \varepsilon$, with $t > t_0$. In KS language trajectory translates into fundamental manifold. In order to extend the definition of Lyapunov stability accordingly an adequate metric d to measure the distance between manifolds is required.

Let Γ_1 and Γ_2 be two (distinct) fundamental manifolds. The fibers in Γ_1 can never intersect the fibers in Γ_2. But both manifolds may share certain fibers, corresponding to the points of intersection between the two resulting trajectories in Cartesian space. The distance between the manifolds at $t \equiv t(s_1) = t(s_2)$ is the distance between the corresponding fibers. Setting θ to a reference value θ_{ref} in Eq. (12) so that $\theta_1 = \theta_2 \equiv \theta_{\mathrm{ref}}$, we introduce the metric:

$$d(t;\Gamma_1,\Gamma_2) = \frac{1}{2\pi}\int_0^{2\pi} \|\mathbf{w}_1(s_1;\vartheta) - \mathbf{w}_2(s_2;\vartheta)\|\,\mathrm{d}\vartheta \tag{19}$$

with $d(t;\Gamma_1,\Gamma_2) \equiv d(\mathcal{F}_1,\mathcal{F}_2)$. It is measured by computing the distance between points in Γ_1 and Γ_2 with the same value of ϑ, and then integrating over the entire fiber. It is defined for given values of physical time, and not fictitious time. The reason is that the goal of this section is to define a theory of stability such that the fundamental manifold inherits the stability properties of the trajectory in Cartesian space. This theory is based on the physics of the system, not affected by a reformulation of the equations of motion.

Consider a fundamental manifold Γ, referred to a nominal trajectory $\mathbf{r}(t)$, and a second manifold Γ^* corresponding to a perturbed trajectory $\mathbf{r}^*(t)$. If the nominal trajectory is Lyapunov stable, then for every $\varepsilon_u > 0$ there is a number $\delta_u > 0$ such that

$$d(t_0;\Gamma,\Gamma^*) < \delta_u \implies d(t;\Gamma,\Gamma^*) < \varepsilon_u.$$

If the initial separation between the manifolds is small it will remain small according to the metric defined in Eq. (19).

The nominal solution $\mathbf{r}(t)$ is said to be asymptotically stable if $\|\mathbf{r}(t) - \mathbf{r}^*(t)\| \to 0$ for $t \to \infty$. Similarly, the fundamental manifold Γ will be asymptotically stable if $d(t;\Gamma,\Gamma^*) \to 0$ for sufficiently long times. The opposite behavior $d(t;\Gamma,\Gamma^*) \to \infty$ corresponds to an asymptotically unstable fundamental manifold. It behaves as if it were asymptotically stable if the time is reversed.

Poincaré maps and orbital stability The notion of Poincaré (or orbital) stability is particularly relevant when analyzing the fundamental manifold due to its geometric implications. Kepler's problem is unstable in the sense of Lyapunov but it is orbitally stable: disregarding the time evolution of the particles within their respective orbits, the separation between the orbits remains constant.

The definition of the Poincaré map in $\mathbb{E}^3$ involves a 2-dimensional section Σ that is transversal to the flow. Denoting by $\mathbf{p}_1, \mathbf{p}_2, \ldots$ the successive intersections of a periodic orbit with Σ, the Poincaré map $\mathscr{P}$ renders

$$\mathscr{P}(\mathbf{p}_n) = \mathbf{p}_{n+1}.$$

The generalization of the Poincaré section to KS space $\mathscr{K} : \Sigma \to \Sigma_u$ results in a subspace embedded in $\mathbb{U}^4$. We showed that the trajectories intersect the fibers at right angles, provided that the velocity $\mathbf{u}'$ is orthogonal to the vector tangent to the fiber. Thus, every fiber defines a section that is transversal to the flow. The transversality condition for Σ translates into the section containing the fiber at $\mathbf{u}$.

The Poincaré section Σ_u can be constructed by combining the set of fibers that are KS transformed to points in Σ. Let $\mathbf{n} = (n_x, n_y, n_z)^\top$ be the unit vector normal to Σ in $\mathbb{E}^3$, projected onto an inertial frame. The Poincaré section takes the form

$$\Sigma \equiv n_x(x - x_0) + n_y(y - y_0) + n_z(z - z_0) = 0 \tag{20}$$

where (x_0, y_0, z_0) are the coordinates of the first intersection point. Equation (20) can be written in parametric form as $\Sigma(x(\eta,\xi), y(\eta,\xi), z(\eta,\xi))$, with η and ξ two free parameters. The extended Poincaré section Σ_u is obtained by transforming points on Σ to KS space and then mapping the fibration $\mathscr{R}$:

$$\Sigma_u = (\mathscr{R} \circ \mathscr{K}^{-1})(\Sigma).$$

The choice of the Poincaré section Σ is not unique, and therefore the construction of Σ_u is not unique either. The resulting Poincaré section Σ_u is a subspace of dimension three embedded in $\mathbb{U}^4$. Indeed, the transformation $(\mathscr{R} \circ \mathscr{K}^{-1})(\Sigma)$ provides:

$$\Sigma \mapsto \Sigma_u(u_1(\eta,\xi,\vartheta), u_2(\eta,\xi,\vartheta), u_3(\eta,\xi,\vartheta), u_4(\eta,\xi,\vartheta))$$

meaning that points in Σ_u are fixed by three parameters, (η, ξ, ϑ). The dimension is raised by $(\mathscr{R} \circ \mathscr{K}^{-1})$.

The intersection between a given fundamental manifold and the Poincaré section Σ_u results in a fiber,

$$\Gamma \cap \Sigma_u = \mathcal{F}.$$

Successive intersections can be denoted $\mathcal{F}_1, \mathcal{F}_2, \ldots$. The Poincaré map in $\mathbb{U}^4$, $\mathscr{P} : \Sigma_u \to \Sigma_u$, is

$$\mathscr{P}(\mathcal{F}_n) = \mathcal{F}_{n+1}.$$

Every point in a fiber intersects Σ_u simultaneously. Due to the $\mathscr{R}$-invariance of the Sundman transformation the time period between crossings is the same for every trajectory connecting $\mathcal{F}_n$ and $\mathcal{F}_{n+1}$.

Let Γ denote a fundamental manifold representing a nominal periodic orbit, and let Γ^* be a perturbed solution. They differ in the conditions at the first Σ-crossing, $\mathcal{F}_1$ and $\mathcal{F}_1^*$ respectively. The manifold Γ is said to be Poincaré (or orbitally) stable if

$$d(\mathcal{F}_1^*, \mathcal{F}_1) < \delta_u \implies d(\mathscr{P}^n(\mathcal{F}_1^*), \mathcal{F}_1) < \varepsilon_u.$$

If the separation between the fibers at the first crossing is small, the separation will remain small after n crossings.

ORDER AND CHAOS

In the previous section we generalized the key concepts of dynamical stability to KS space. The approach we followed aims for a theory that captures the physical properties of the system, instead of focusing on its purely numerical conditioning. The next step is the analysis of chaos in $\mathbb{U}^4$.

Chaotic systems are extremely sensitive to numerical errors due to the strong divergence of the integral flow. This is specially important in the vicinity of singularities, and it is precisely here where KS regularization exhibits all its potential. This section focuses on characterizing the exponential divergence of trajectories in $\mathbb{U}^4$ due to highly unstable dynamics.

By definition the fundamental manifold is mapped to a trajectory in $\mathbb{E}^3$. The equations of motion in $\mathbb{U}^4$ are no more than a reformulation of a dynamical system originally written in $\mathbb{E}^3$. For sufficiently smooth perturbations the Picard-Lindelöf theorem ensures the uniqueness of the solution. Thus, the corresponding fundamental manifold is also unique and its KS transform defines only one trajectory. This means that any trajectory in the fundamental manifold is mapped to the same exact trajectory in $\mathbb{E}^3$, no matter the position within the initial fiber. An observer in three-dimensional space, unaware of the extra degree of freedom introduced by the gauge $\mathscr{R}$, will always perceive the same trajectory no matter the values of ϑ.

The $\mathscr{K}$-separation

In order to integrate the equations of motion numerically in $\mathbb{U}^4$ the initial values of $\mathbf{u}_0$ and $\mathbf{u}_0'$ need to be fixed. This means choosing a point in the fiber $\mathcal{F}_0$. Since all the points in $\mathcal{F}_0$ are KS transformed to the same exact state vector in $\mathbb{E}^3$, the selection of the point is typically arbitrary. But for an observer in $\mathbb{U}^4$ different values of ϑ yield different initial conditions, and therefore the

initial value problem to be integrated may behave differently. Ideally* all trajectories emanating from $\mathcal{F}_0$ remain in the same fundamental manifold, that is unique. However, numerical errors leading to the exponential divergence of the trajectories can cause the trajectories to depart from the fundamental manifold. In other words, after sufficient time two trajectories originating from the same fiber $\mathcal{F}_0$, $\mathbf{w}_0 = \mathscr{R}(\vartheta; \mathbf{u}_0)$, will no longer define the same fiber $\mathcal{F}(s)$, $\mathbf{w}(s) \neq \mathscr{R}(\vartheta; \mathbf{u}(s))$. In this case Thm. 1 will be violated. Multiple fundamental manifolds will appear, obtained by mapping the transformation $\mathscr{R}$ over each of the trajectories. The observer in $\mathbb{E}^3$ will see a collection of trajectories that depart from the same exact state vector and they separate in time, as if the problem had a random component. This behavior can only be understood in four dimensions.

These topological phenomena yield a natural way of measuring the error growth in KS space without the need of a precise solution. Let $\mathbf{u}(s)$ be a reference trajectory in $\mathbb{U}^4$, and let $\mathbf{w}(s)$ be a second trajectory defined by $\mathbf{w}_0 = \mathscr{R}(\vartheta; \mathbf{u}_0)$. It is possible to build the fundamental manifold Γ from the solution $\mathbf{u}(s)$. The second solution is expected to be $\mathbf{w}^*(s) = \mathscr{R}(\vartheta; \mathbf{u}(s))$ by virtue of Thm. 1. When numerical errors are present $\mathbf{w}(s)$ and its expected value $\mathbf{w}^*(s)$ (the projection of the fundamental manifold) may not coincide. Note that $\mathbf{w}(s) = \mathbf{w}^*(s)$ ensures the uniqueness of the solution, but says nothing about its accuracy. The separation between $\mathbf{w}(s)$ and its projection on Γ is an indicator of the breakdown of the topological structure supporting the KS transformation, meaning that the solutions can no longer be trusted.

Motivated by this discussion we introduce the concept of the $\mathscr{K}$-separation,

$$d_{\mathscr{K}}(s) = \|\mathbf{w}(s) - \mathbf{w}^*(s)\| = \|\mathbf{w}(s) - \mathscr{R}(\vartheta; \mathbf{u}^*(s))\| \tag{21}$$

defined as the Euclidean distance between an integrated trajectory and its projection on the manifold of solutions. Monitoring the growth of the $\mathscr{K}$-separation is a way of quantifying the error growth of the integration. In the context of N-body simulations, Quinlan and Tremaine[13] discussed how the separation between nearby trajectories evolves: the divergence is exponential in the linear regime when the separation is small, but the growth rate is reduced when the separation is large. At this point the separation might be comparable to the interparticle distance. The $\mathscr{K}$-separation will grow exponentially at first (for $d_{\mathscr{K}} \ll 1$) until it is no longer small ($d_{\mathscr{K}} \sim \mathcal{O}(1)$), and then its growth slows down. Locating the transition point is equivalent to finding the time scale $t_{\rm cr}$ in which the solution in KS space can no longer be trusted: for $t < t_{\rm cr}$ the topological structure of $\mathbb{U}^4$ is preserved, but for $t > t_{\rm cr}$ the uniqueness of the manifold of solutions Γ is not guaranteed.

For $t < t_{\rm cr}$ the $\mathscr{R}$-invariance of the Sundman transformation holds. The time for all the points in a fiber coincides. Thus, $t_{\rm cr}$ and $s_{\rm cr}$ are interchangeable: at $t < t_{\rm cr}$ it is also $s < s_{\rm cr}$. The behavior of the solutions can be equally analyzed in terms of the physical or the fictitious time. In practice the $\mathscr{K}$-separation is evaluated following the steps in the second section of the paper.

Topological stability

The uniqueness of Γ can be understood as *topological stability*. KS space is said to be topologically stable if all the trajectories emanating from the same fiber define a unique manifold of solutions, and therefore they are all KS-transformed to the same trajectory in $\mathbb{E}^3$. For an observer

*Due to the limited precision of floating point arithmetic, even the fact that all points generated with Eq. (14) and varying ϑ will be KS-transformed to the same exact point in $\mathbb{E}^3$ should be questioned. The loss of accuracy in the computation of the initial conditions in $\mathbb{U}^4$ will eventually introduce errors of random nature. As a result, Eq. (14) provides points that are not exactly in the true fiber. Although the separation is small (of the order of the round-off error) and negligible in most applications, it may have an impact on the numerical integration of chaotic systems.

in $\mathbb{E}^3$ a topologically unstable system seems non-deterministic, with solutions departing from the same initial conditions but separating in time with no apparent reason.

A system is topologically stable in the interval $t < t_{\text{cr}}$. The trajectories diverge exponentially,

$$d_{\mathscr{K}}(t)/d_{\mathscr{K}}(0) \sim \mathrm{e}^{\gamma_t t} \qquad \text{or} \qquad d_{\mathscr{K}}(s)/d_{\mathscr{K}}(0) \sim \mathrm{e}^{\gamma_s s}.$$

Here γ is equivalent to a Lyapunov exponent. For $t > t_{\text{cr}}$ this equation no longer models the growth of the $\mathscr{K}$-separation and the system is topologically unstable. Simulations over the transition time t_{cr} integrated in $\mathbb{U}^4$ can no longer be trusted. Depending on the integrator, the integration tolerance, the floating-point arithmetic, the compiler, etc. the values of t_{cr} for a given problem might change. Thus, topological stability is a property of a certain propagation, which requires all the previous factors to be defined.

The validity of the solution for an integration over the critical time t_{cr} is not guaranteed. When $t_{\text{cr}} < t_{\text{esc}}$ (with t_{esc} denoting the escape time) not even the value of t_{esc} can be estimated accurately. In such a case solutions initialized at different points in the fiber may yield different escape times.

The method presented in this section provides an estimate of the interval in which the propagation is topologically stable. The exponent γ depends on the integration scheme and the dynamics, but it is not strongly affected by the integration tolerance. An estimate of the value of γ provides an estimate of the critical time for a given integration tolerance ε. Assuming $d_{\mathscr{K}}(t_{\text{cr}}) \sim 1$:

$$t_{\text{cr}} \sim -\frac{1}{\gamma_t} \log \varepsilon \tag{22}$$

Conversely, if the simulation needs to be carried out up to a given t_f, the required integration tolerance is approximately

$$\varepsilon \sim \mathrm{e}^{-\gamma_t t_f} \tag{23}$$

This simple criterion proves useful for tuning and evaluating the numerical integration. In the following examples of application the values of γ_t are estimated by finding the slope of the exponential growth of the $\mathscr{K}$-separation in logarithmic scale. Although more rigorous algorithms could be developed, this approximation provides a good estimate of transition time between regimes.

THE ALGORITHM

From a practical point of view, the main concept behind topological stability is the $\mathscr{K}$-separation, $d_{\mathscr{K}}$. This separation relates to how well the structure supporting the KS transformation is preserved. In a nutshell, large $\mathscr{K}$-separations are caused by large numerical errors. As we will prove in the next section of the paper, it is a good indicator of the global numerical error. It is computed as follows:

1. Transform the initial conditions $\mathbf{r}_0$ and $\mathbf{v}_0$ to KS coordinates ($\mathbf{u}_0$ and $\mathbf{u}_0'$) using Eqs. (12), (13) and (15). Set θ to an arbitrary value θ_1, for example $\theta_1 = 0$.

2. Propagate the orbit in KS coordinates $\mathbf{u}(s)$ starting from $\mathbf{u}_0$ and $\mathbf{u}_0'$.

3. Repeat step 1 to generate a second set of initial conditions in KS space, $(\mathbf{w}_0, \mathbf{w}_0')$, by setting $\theta = \theta_2$ in Eq. (12). Make $\theta_2 \neq \theta_1$ and not too close to each other, e.g. $\theta_2 = \pi/2$.

4. Propagate the orbit $\mathbf{w}(s)$ from $\mathbf{w}_0$ and $\mathbf{w}_0'$.

5. The $\mathscr{K}$-separation at each step s is simply

$$d_{\mathscr{K}}(s) = \|\mathbf{w}(s) - \mathbf{R}(\vartheta)\mathbf{u}(s)\|,$$

with $\vartheta = \theta_2 - \theta_1$. Matrix $\mathbf{R}$ is defined in Eq. (7).

The problem is typically normalized so the initial radius equals one. Therefore, $d_{\mathscr{K}}$ actually relates to the relative error. At first it will be comparable to the machine zero, and it will grow in time as errors accumulate. When it becomes of order one it means that the magnitude of the errors are comparable to the characteristic size of the orbit.

QUANTIFYING NUMERICAL ERRORS

The present section shows how monitoring topological stability is useful for quantifying global errors. Four examples will be analyzed:

1. A geocentric orbit strongly perturbed by lunar close-encounters.
2. An orbiter in the Jovian system perturbed by Io, Europa, Ganymede and Callisto.
3. The Pythagorean three-body problem.
4. A symmetric configuration of the 8-body problem.

Problems 3 and 4 will be propagated using Heggie-Mikkola's regularization of the N-body problem based on the KS transformation.[14,15]

Problem 1: Resonant encounters with the Moon

Problem 1 models the orbit of a particle perturbed by a realistic force model. First, the gravitational attraction of the Moon, using the DE431 ephemeris solution. Second, atmospheric drag. The atmospheric density is approximated by an exponential model, with $C_D = 2$, and $A/m = 0.05$ m^2/kg. Third, solar radiation pressure ($C_R = 1.2$) accounting for seasonal variations. Fourth, a non-uniform terrestrial gravity field given by a 10×10 grid of harmonics from the GGM03S model. The osculating elements at the initial epoch can be found in Table 1.

a [km]	e	i [°]	ω [°]	Ω [°]	M_0 [°]
340000	0.9373	3.1967	314.0441	311.5561	6.1920

Table 1: **Definition of the test orbit in the ICRF/J2000 frame with the Earth mean equator at epoch as the reference plane (JD 2456900)**

The high eccentricity of the orbit brings its apoapsis very close to the orbit of the Moon, while keeping periapsis low so atmospheric drag and high-order terms of the gravity field still perturb the orbit significantly. Moreover, the relative phasing with respect to the Moon is such that the particle suffers from several close encounters with the Moon. These encounters modify the energy and inclination of the orbit significantly in the 4-year time span that we considered (~65 revs). As a result, the orbit is extremely sensitive to numerical errors. Figure 4 shows the orbit.

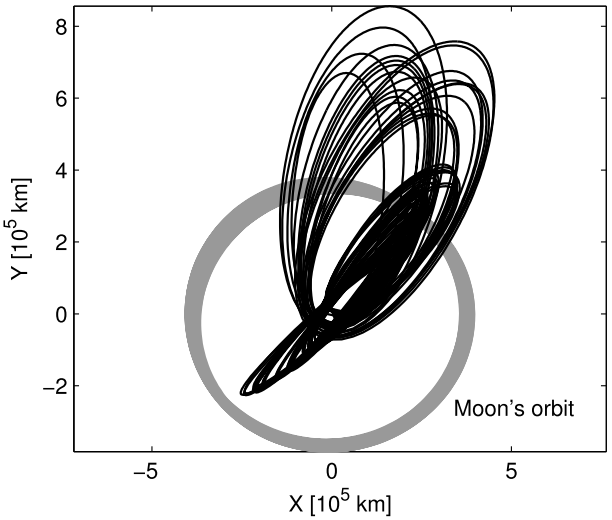

Figure 4: **Geocentric orbit strongly perturbed by several close encounters with the Moon**

The error in position, plotted in Fig. 5, is measured by comparing the solution with a very accurate propagation using quadruple-precision floating-point arithmetic. In order to generate the reference solution, the tolerances for the integrator are set to 10^{-21}, five orders of magnitude below the machine zero in double precision. In this case, the orbit is propagated using LSODAR. The error grows exponentially and becomes comparable to the initial semimajor axis of the orbit after roughly 3.5 years. Estimating this *e*-folding time is critical because results beyond this point are shadowed by numerical errors. In some applications dealing with chaotic systems the results are only meant to provide statistical insight into the solution, and admit propagations over the *e*-folding time. However, in our case we aim to represent the orbit of the particle as accurately as possible, and errors comparable to the characteristic size of the orbit are not admissible.

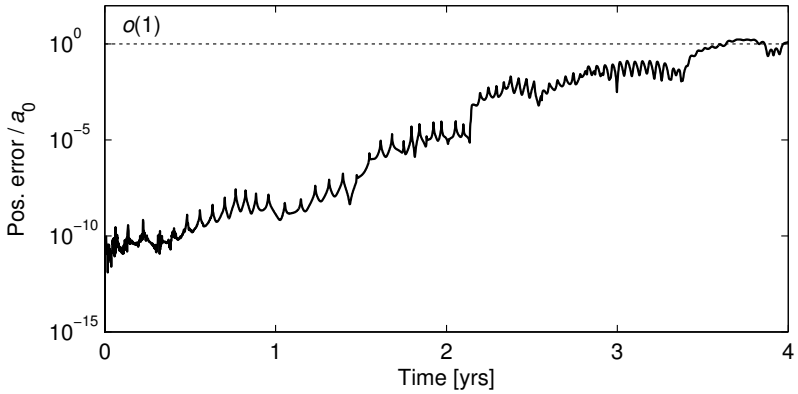

Figure 5: **Error in position for Problem 1**

Although running the propagator in quadruple-precision floating-point arithmetic might provide an accurate measure of the errors, it is certainly not a practical technique: some Fortran compilers support extended precision, but other languages such as Matlab or Python do not support this arithmetic. The new method presented in this paper works in double precision, and it is able to cap-

ture the evolution of the error and the e-folding time accurately; the evolution of the $\mathscr{K}$-separation displayed in Fig. 6 also estimates that after 3.5 years the errors will be comparable to the size of the orbit. Moreover, the qualitative evolution of the $\mathscr{K}$-separation is a good representation of how errors evolve in Fig. 5.

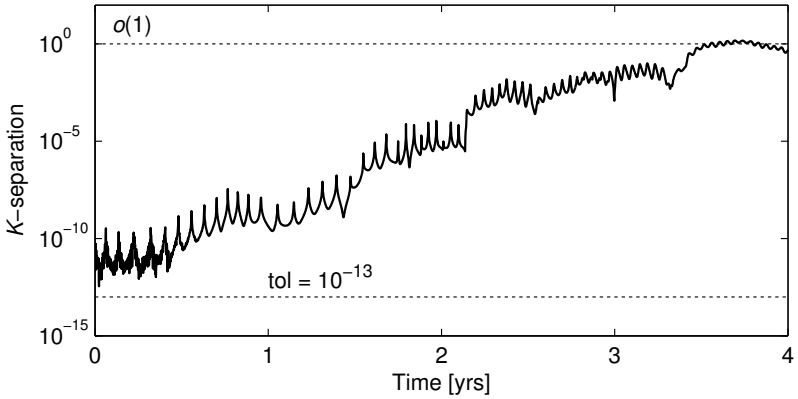

Figure 6: **$\mathscr{K}$-separation in the integration of the geocentric orbit**

Problem 2: Jupiter system

Inspired by the Europa mission, the second problem considers a spacecraft orbiting around Jupiter and subject to the attraction from Io, Europa, Ganymede, and Callisto. The orbits of the moons are assumed circular and coplanar. The initial orbit of the spacecraft is almost circular ($e = 0.08$), with a semimajor axis of approximately 613,000 km. The inclination relative to the orbital plane of the moons is just 0.5°.

Figure 7 shows how the semimajor axis and eccentricity evolve in time. This particular orbit experiences several close encounters with Europa, responsible for the sequence of apoapsis raising and lowering events. In particular, the apoapsis of the orbit changes by almost 30% of the initial radius, due to significant changes in the eccentricity of the orbit. The orbit of the spacecraft is propagated for 4 years, which corresponds to more than 450 orbits, using a Dormand-Prince 5(4) integrator.

The evolution of the $\mathscr{K}$-separation (Fig. 8) shows that, for the current integration setup, 1.25 years into the propagation the numerical error dominates the solution. Results beyond this point cannot be trusted if the exact path of the spacecraft is to be tracked.

Problem 3: Pythagorean three-body problem

Problem 3 corresponds to a classical problem in N-body simulations: the Pythagorean three-body problem. Three bodies with masses $m_1 = 3$, $m_2 = 4$, and $m_3 = 5$ form a triangle with vertices $\mathbf{r}_1 = (1, 3, 0)$, $\mathbf{r}_2 = (-2, -1, 0)$, and $\mathbf{r}_3 = (1, -1, 0)$, starting with zero velocity. This problem is an interesting reference that has been studied widely in the past.[16] The solution, integrated using the Bulirsch-Stoer extrapolation scheme, is presented in Fig. 9. Two of the particles (1,3) end up forming a binary that escape toward the bottom-left corner, whereas particle 2 is ejected toward the top-right corner.

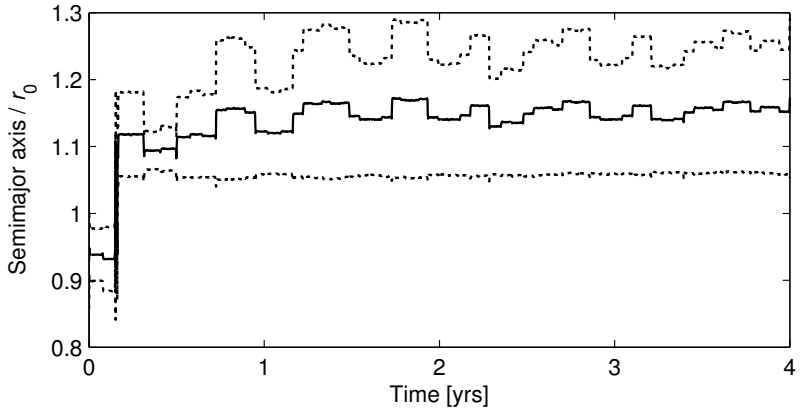

(a) Semimajor axis (dashed lines correspond to periapsis and apoapsis)

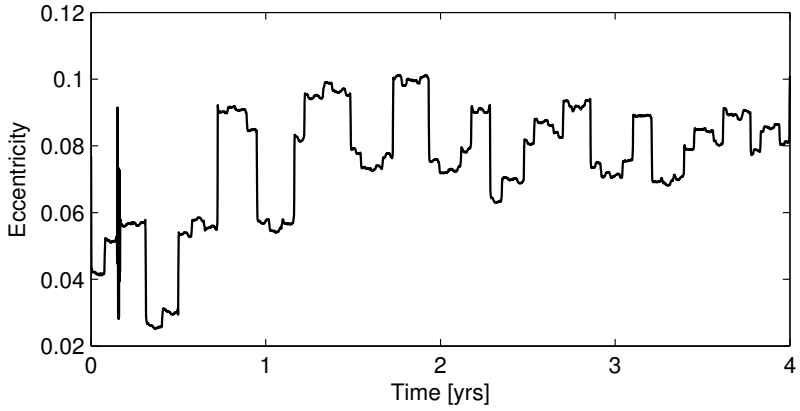

(b) Eccentricity

Figure 7: **Evolution of the orbital elements of the Jupiter orbiter**

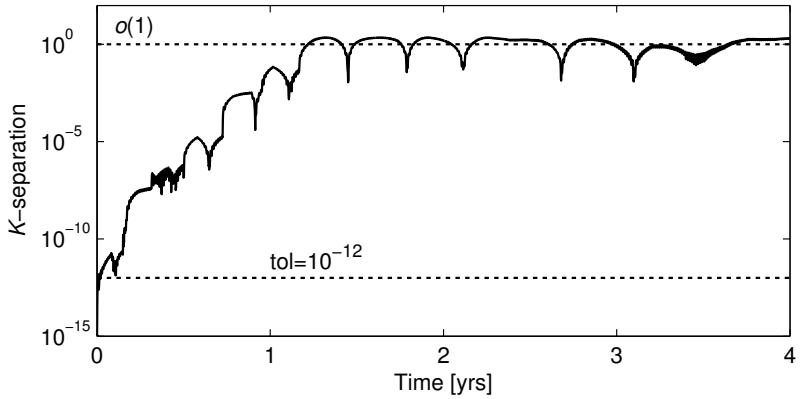

Figure 8: $\mathscr{K}$ **-separation for the Jupiter orbiter**

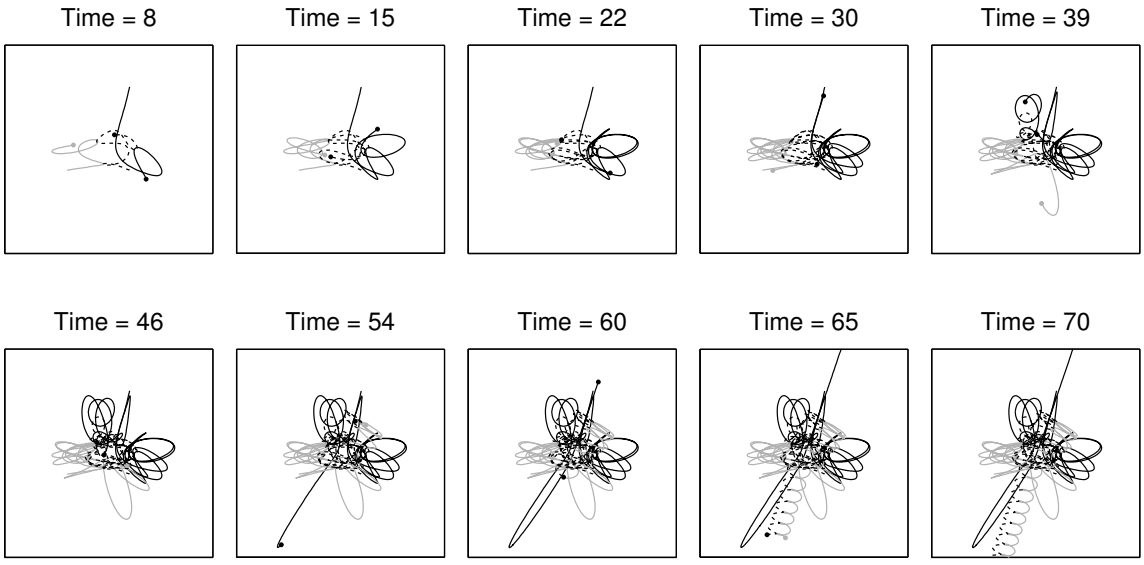

Figure 9: **Solution to the Pythagorean three-body problem**

Encounters are not too strong in this case, and the integration is not problematic. The $\mathscr{K}$-separation, presented in Fig. 10, shows that the integration time ($t = 70$) is well below the e-folding time; the errors by the end of the integration are small compared to the size of the orbit. Therefore, the current integration setup adequately captures the dynamics beyond the escape time.

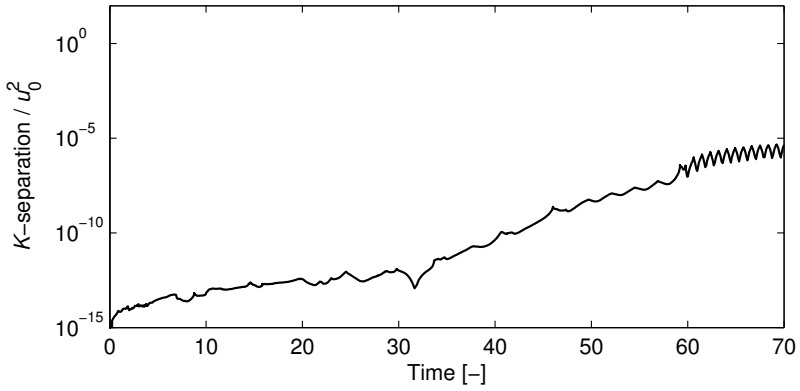

Figure 10: **$\mathscr{K}$-separation for the Pythagorean three-body problem**

8-body problem

The fourth problem consists in eight bodies of unit mass that initially form a cube of side 2. They have velocities equal to one, directed in counter-clockwise direction. Figure 11 shows the solution obtained by initializing the problem in KS space using $\theta = 0$, and Fig. 12 depicts the solution obtained with $\theta = 270°$.

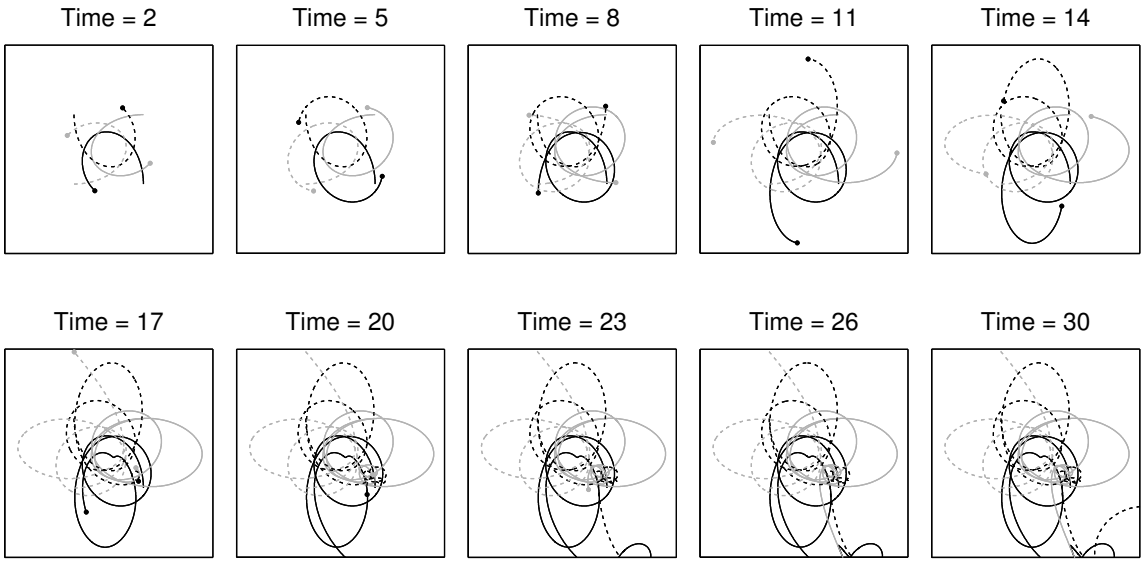

Figure 11: **Solution to the 8-body problem with** $\theta = 0$

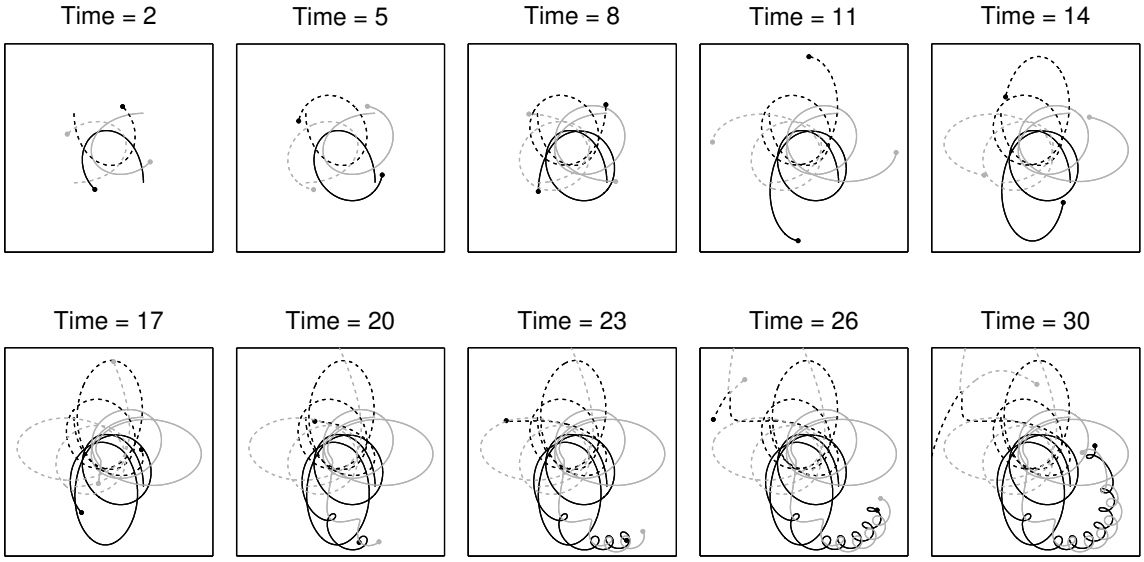

Figure 12: **Solution to the 8-body problem with** $\theta = 270°$

At $t = 17$ the difference between the solutions is noticeable. This is approximately the e-folding time predicted by the evolution of the $\mathscr{K}$-separation in Fig. 13. The symmetry of the problem is lost, as numerical errors shadow the true solution. The particles shown in Fig. 11 escape at approximately $t \sim 25$, whereas in Fig. 12 the system remains bounded.

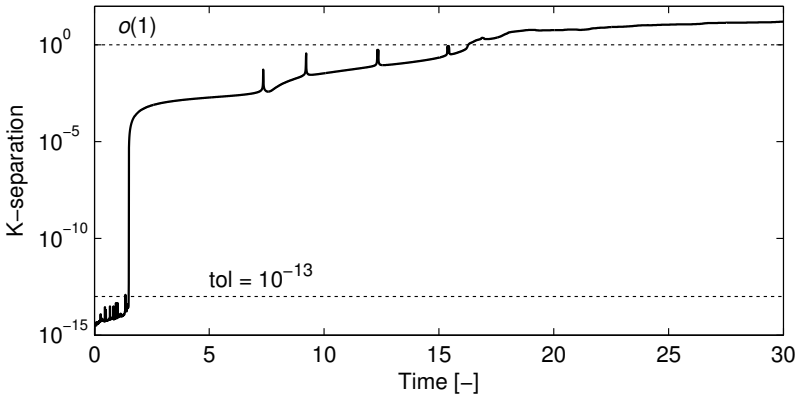

Figure 13: $\mathscr{K}$ **-separation for the 8-body problem**

Interestingly, the energy is conserved down to $10^{-10}E_0$ during almost the entire integration. The error grows at first after the a sequence of encounters, and then it remains stable at the reported level. The integrator preserves the energy well, although the solutions are not accurate enough at the end of the integration. Monitoring the change in the energy fails to predict the actual evolution of the global error, whereas the new method captures it. This is a clear example of the fact that the energy being conserved is a necessary but not sufficient condition for solutions to be accurate.

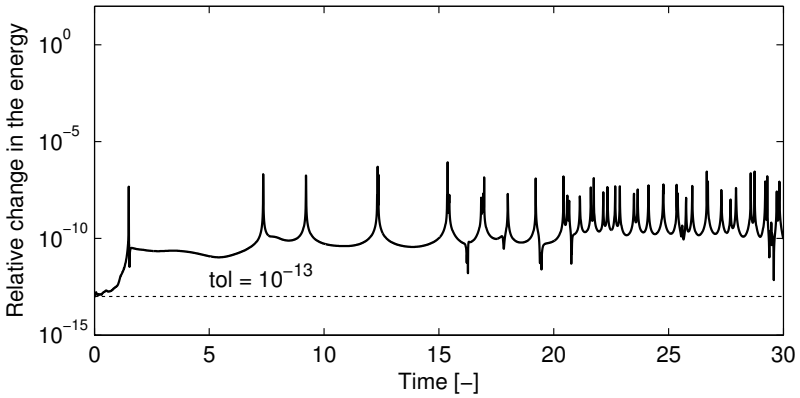

Figure 14: **Conservation of the energy**

CONCLUSIONS

The extra degree of freedom introduced by the Kustaanheimo-Stiefel transformation imposes specific constraints on the numerical propagation of an orbit. But numerical errors might violate such constraints, destroying the topological support of KS regularization. As a result, and after translating classical concepts of stability to KS language, it follows a new metric for assessing numerical integration errors.

The method can be used for evaluating whether the current integration setup is well tuned for solving the problem, or if the solution is not accurate enough. Similarly, it can be used to estimate what kind of integration tolerance (or step size) should be used for a particular problem.

ACKNOWLEDGMENTS

This research was carried out at the Jet Propulsion Laboratory, California Institute of Technology, under a contract with the National Aeronautics and Space Administration.

REFERENCES

[1] P Kustaanheimo and E Stiefel. Perturbation theory of Kepler motion based on spinor regularization. *Journal für die reine und angewandte Mathematik*, 218:204–219, 1965.

[2] Heinz Hopf. Über die Abbildungen der dreidimensionalen Sphäre auf die Kugelfläche. *Mathematische Annalen*, 104(1):637–665, 1931.

[3] Karl F Sundman. Mémoire sur le problème des trois corps. *Acta Mathematica*, 36(1):105–179, 1913.

[4] K Zare and V Szebehely. Time transformations in the extended phase-space. *Celestial Mechanics*, 11(4):469–482, 1975.

[5] Javier Roa. *Regularization in Astrodynamics: applications to relative motion, low-thrust missions, and orbit propagation*. PhD thesis, Technical University of Madrid, September 2016.

[6] Eduard L. Stiefel and Gerhard Scheifele. *Linear and regular Celestial Mechanics*. Springer-Verlag, New York, Heidelberg, Berlin, 1971.

[7] J Baumgarte. Numerical stabilization of the differential equations of Keplerian motion. *Celestial Mechanics*, 5(4):490–501, 1972.

[8] J Baumgarte. Stabilized Kepler motion connected with analytic step adaptation. *Celestial Mechanics*, 13(1):105–109, 1976.

[9] Hideyoshi Arakida and Toshio Fukushima. Long-term integration error of Kustaanheimo-Stiefel regularized orbital motion. *The Astronomical Journal*, 120(6):3333, 2000.

[10] Javier Roa, Hodei Urrutxua, and Jesús Peláez. Stability and chaos in Kustaanheimo-Stiefel space induced by the Hopf fibration. *Monthly Notices of the Royal Astronomical Society*, 459(3):2444–2454, 2016.

[11] Javier Roa and Jesús Peláez. The theory of asynchronous relative motion i: time transformations and nonlinear corrections. *Celestial Mechanics and Dynamical Astronomy*, 127(3):301–330, 2017.

[12] Javier Roa and Jesús Peláez. The theory of asynchronous relative motion ii: universal and regular solutions. *Celestial Mechanics and Dynamical Astronomy*, 127(3):343–368, 2017.

[13] Gerald D Quinlan and Scott Tremaine. On the reliability of gravitational N-body integrations. *Monthly Notices of the Royal Astronomical Society*, 259(3):505–518, 1992.

[14] Douglas C Heggie. A global regularisation of the gravitational N-body problem. *Celestial Mechanics*, 10(2):217–241, 1974.

[15] Seppo Mikkola. A practical and regular formulation of the N-body equations. *Monthly Notices of the Royal Astronomical Society*, 215(2):171–177, 1985.

[16] Victor Szebehely and C Frederick Peters. Complete solution of a general problem of three bodies. *The Astronomical Journal*, 72:876, 1967.